Complete spectral characterization of biphotons by simultaneously determining their frequency sum and difference in a single quantum interferometer

Baihong Li (李百宏),[1,*] Changhua Chen (陈昌花),[1] Xiao Xiang (项晓),[2] Runai Quan (权润爱),[1]
Ruifang Dong (董瑞芳),[2,†] Shougang Zhang (张首刚),[2] Xiangying Hao (郝向英),[3] and Rui-Bo Jin (金锐博)[3,‡]
[1]*Department of Physics, Shaanxi University of Science and Technology, Xi'an 710021, China*
[2]*Key Laboratory of Time and Frequency Primary Standards, National Time Service Center, Chinese Academy of Sciences, Xi'an 710600, China*
[3]*Hubei Key Laboratory of Optical Information and Pattern Recognition, Wuhan Institute of Technology, Wuhan 430205, China*

(Received 6 June 2023; accepted 28 July 2023; published 14 August 2023)

We propose theoretically a quantum interferometer in which the NOON state interferometer is combined with the Hong-Ou-Mandel interferometer. With this interferometer, the temporal interference patterns associated with biphoton frequency sum and difference can be shown in different parts of a single interferogram. It is thus possible to simultaneously obtain the spectral correlation information of biphotons in both frequency sum and difference by taking the Fourier transform from such an interferogram. This provides a method for complete spectral characterization of an arbitrary two-photon state with exchange symmetry and might be useful in quantum Fourier-transform spectroscopy where direct spectral measurement is difficult. Furthermore, as it can realize the measurement of time intervals on three scales at the same time, we expect that it can provide a method in quantum metrology. Finally, we discuss another potential application of such an interferometer in the generation and characterization of high-dimensional and phase-controlled frequency entanglement.

DOI: 10.1103/PhysRevA.108.023713

I. INTRODUCTION

Quantum interferometry [1], the heart of various quantum technology applications, can be realized by different quantum interferometer such as the Hong-Ou-Mandel interferometer (HOMI) [2,3] and the NOON state interferometer (NOONI) [4]. These interferometers have been used to demonstrate various nonclassical features of entangled photons such as the violation of Bell's inequality [5] and dispersion cancellation [6–8]. The HOMI has many important applications in quantum information science, e.g., quantum communication [9], quantum computing [10], quantum imaging [11,12], and quantum metrology [13–15]. The NOONI has been widely used in quantum lithography [4,16], quantum high-precision measurement [17–19], quantum microscopy [20–22], error correction [23], and so on.

It is well known that using the interferometric spectrometer technology established by the Wiener–Khinchin theorem in classical optics, it is possible to extract the spectral information of light by making a Fourier transform on its time-domain interferograms obtained from Mach-Zehnder or Michelson interferometers. Jin *et al.* [24–26] extended the Wiener-Khinchin theorem to a quantum version where the biphoton spectral information of frequency difference and frequency sum between signal and idler photons can be extracted by applying a Fourier transform on the time-domain patterns of the HOMI and NOONI, respectively. This can be considered as a kind of quantum Fourier-transform spectroscopy. However, the HOMI only depends on the frequency difference, and the NOONI only depends on the frequency sum, making these two interferometers access only one-dimensional (1D) information in frequency difference or frequency sum, which is mismatched with two-photon states in two dimensions [24,27]. To solve this problem, Abouraddy *et al.* [28] theoretically proposed a linear two-photon interferometer containing two independent delays, but it is relatively hard to realize in an experiment. Alternatively, a two-dimensional (2D) joint spectral intensity (JSI) associated with the frequency sum and difference and its Fourier transform, joint temporal intensity (JTI), associated with the time difference and sum can be obtained directly in an experiment, but it is rather challenging and impractical, especially for the broadband spectrum [29,30]. A comparative study of various different techniques on spectral characterization of biphotons, as well as their relative advantages and disadvantages can be found in Ref. [31].

In this paper, we propose a type of quantum interferometer in which the NOONI is combined with the HOMI. This interferometer depends on both frequency sum and frequency difference and combines the advantages of both the NOONI and the HOMI into a single interferometer. The temporal interference patterns associated with biphoton frequency sum and difference can be shown in different parts of a single interferogram. It can thus simultaneously obtain the spectral correlation information of biphotons both in frequency sum and frequency by taking the Fourier transform of the time-domain quantum interferograms obtained from

*li-baihong@163.com
†dongruifang@ntsc.ac.cn
‡jin@wit.edu.cn

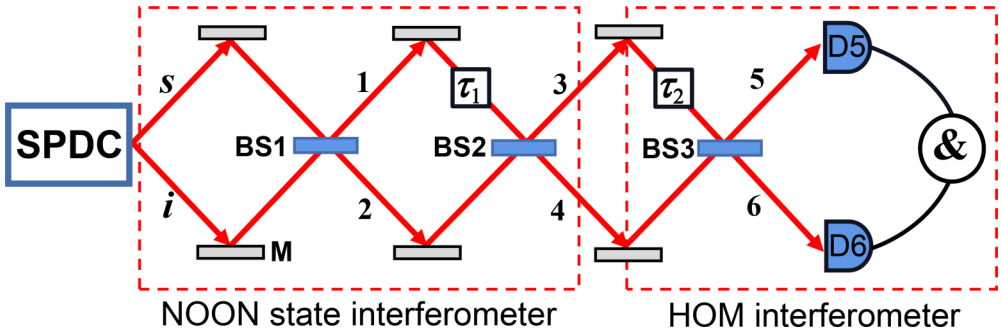

FIG. 1. Schematic diagram of the proposed quantum interferometer. It can be considered as a combination of the NOON state interferometer (the left part) and the HOM interferometer (the right part). M: Mirror, BS: beam splitter, D: detector, &: coincidence count.

such an interferometer. This may be especially useful for quantum Fourier-transform spectroscopy where direct spectral measurement is difficult. The specific interferograms of the interferometer depend on the exchange symmetry of the biphoton and the ratio between the width of frequency difference and frequency sum, which correspond to different types of frequency entangled resources, such as frequency correlated, uncorrelated, or anticorrelated. Therefore, the proposed interferometer can be used for complete spectral characterization of an arbitrary two-photon state with exchange symmetry. Moreover, as it can realize the measurement of time intervals on three scales at the same time, we expect that it can provide a method in quantum metrology. Finally, we discuss another potential application of such an interferometer in the generation and characterization of high-dimensional and phase-controlled frequency entanglement.

The rest of the paper is organized as follows: In Sec. II, we describe the setup of the proposed interferometer and discuss several interferometric results based on its coincidence count rates derived theoretically from the frequency domain. In Sec. III, we give some typical interferograms of the interferometer for different types of frequency-entangled resources and make a characteristic analysis of the interferometer. In Sec. IV, we compare our results with that of the NOONI and HOMI and discuss potential applications of such an interferometer in quantum Fourier-transform spectroscopy, quantum metrology, generation, and characterization of high-dimensional and phase-controlled frequency entanglement. Section V summarizes the results and concludes the paper.

II. THEORY OF THE COMBINATION INTERFEROMETER

In this part, we propose a quantum interferometer with the setup shown in Fig. 1. To understand better such an interferometer, it can be considered as a combination of the NOONI (the left part) and the HOMI (the right part). The biphotons are generated by the spontaneous parametric down-conversion (SPDC) or spontaneous four-wave-mixing process. As derived in Appendix A, the coincidence count rates between two detectors (D5 and D6) as functions of time delay τ_1 and τ_2 for the combination interferometer can be expressed as

$$R(\tau_1, \tau_2) = \frac{1}{64}\int_0^\infty \int_0^\infty d\omega_s d\omega_i r(\omega_s, \omega_i, \tau), \tag{1}$$

where r is the coincidence probability density, which reads

$$\begin{aligned} r(\omega_s, \omega_i, \tau_1, \tau_2) = |f(\omega_s, \omega_i)(e^{-i\omega_s(\tau_1+\tau_2)} + e^{-i\omega_s\tau_1} + e^{-i\omega_s\tau_2} - 1)(e^{-i\omega_i(\tau_1+\tau_2)} - e^{-i\omega_i\tau_1} - e^{-i\omega_i\tau_2} - 1) \\ + f(\omega_i, \omega_s)(e^{-i\omega_i(\tau_1+\tau_2)} + e^{-i\omega_i\tau_2} - e^{-i\omega_i\tau_1} + 1)(e^{-i\omega_s(\tau_1+\tau_2)} - e^{-i\omega_s\tau_2} + e^{-i\omega_s\tau_1} + 1)|^2, \end{aligned} \tag{2}$$

where $f(\omega_s, \omega_i)$ is the joint spectral amplitude (JSA) of the signal and idler photons. The specific expression of r depends on the symmetry of the JSA. For simplicity, we assume that the JSA is symmetric, i.e., $f(\omega_s, \omega_i) = f(\omega_i, \omega_s)$ in our discussions below. Assuming that $\omega_s = \omega_p/2 + \Omega_s$ and $\omega_i = \omega_p/2 + \Omega_i$, where $\Omega_{s,i}$ is the frequency detuning between the signal (idler) photon and half of the pump center frequency $\omega_p/2$, then Eq. (2) can be expressed as the form of frequency sum $\Omega_+ = \Omega_s + \Omega_i$ and frequency difference $\Omega_- = \Omega_s - \Omega_i$,

$$\begin{aligned} r(\Omega_+, \Omega_-, \tau_1, \tau_2) = 32|f(\Omega_+, \Omega_-)|^2\{1 - \tfrac{1}{2}\cos[(\omega_p + \Omega_+)\tau_1]\cos(\Omega_-\tau_2) - \tfrac{1}{2}\cos[(\omega_p + \Omega_+)\tau_2] - \tfrac{1}{2}\cos(\Omega_-\tau_2) \\ + \tfrac{1}{4}\cos[(\omega_p + \Omega_+)(\tau_2 + \tau_1)] + \tfrac{1}{4}\cos[(\omega_p + \Omega_+)(\tau_2 - \tau_1)]\}. \end{aligned} \tag{3}$$

In general, the JSA cannot be factorized as a product of $f(\omega_s)$ and $f(\omega_i)$. However, $f(\Omega_+, \Omega_-)$ can be factorized as a product of $f_+(\Omega_+)$ and $f_-(\Omega_-)$ in terms of collective coordinate Ω_+ and Ω_-, i.e., $f(\Omega_+, \Omega_-) = f_+(\Omega_+)f_-(\Omega_-)$ [30]. Equation (3) can then be integrated independently with respect to Ω_+ and Ω_-. If we define $F(\Omega_\pm) = |f_\pm(\Omega_\pm)|^2$, its Fourier transform would be

$$G_\pm(\tau) = \frac{1}{\sqrt{2\pi}}\int_{-\infty}^{\infty} F(\Omega_\pm)e^{i\Omega_\pm\tau}d\Omega_\pm. \tag{4}$$

Integrating Eq. (3) over the entire frequency range, it is found that $R(\tau_1, \tau_2)$ can be expressed as functions of $G(\tau)$. We can

thus obtain the normalized coincidence count rates,

$$R_N(\tau_1,\tau_2) = 1 - \tfrac{1}{2}g_+(\tau_1)g_-(\tau_2) - \tfrac{1}{2}g_+(\tau_2) - \tfrac{1}{2}g_-(\tau_2) + \tfrac{1}{4}g_+(\tau_2+\tau_1) + \tfrac{1}{4}g_+(\tau_2-\tau_1), \quad (5)$$

where $g_\pm(\tau) = \mathrm{Re}[G_\pm(\tau)/G_\pm(0)]$. Equation (5) is the central equation of the present paper. It can be seen from Eqs. (3) and (5) that the result of the combination interferometer is determined by both frequency sum and frequency difference, which is quite different from the NOON state interference determined only by the frequency sum and the standard HOM interference determined only by the frequency difference for the symmetric JSA [24,27] (see also Appendix C). In other words, Eq. (5) contains complete spectral information of biphotons associated with both frequency sum and difference, which can be obtained by making a Fourier transform of a single time-domain quantum interferogram obtained from the combination interferometer. Additionally, it can be found that if $\tau_1 = 0$, Eq. (5) will reduce to that of a standard HOM interference [24]. This is because the two beam splitters (BS1 and BS2) play a role of unit transformation matrix, leading to the same output states (3 and 4) as the input (s and i). On the other hand, if $\tau_2 = 0$, the coincidence count rates will always be equal to zero. It means that, whatever τ_1, the two outputs 3 and 4 are indistinguishable. In this case, the output states (3 and 4) are the same as the input states (s and i) except for a global phase introduced by the delay time τ_1, and the global phase does not affect the final result. Thus, the output states 3 and 4 are indistinguishable, resulting in a zero coincidence count at $\tau_2 = 0$ because of destructive interference.

As an example, we take the symmetric JSA as the products of two Gaussian functions, i.e., $f(\Omega_+,\Omega_-) = \exp(-\Omega_+^2/4\sigma_+^2)\exp(-\Omega_-^2/4\sigma_-^2)$, where $\sigma_\pm$ denote the linewidth of two functions determined by the linewidth of pump pulse and the phase-matching condition, respectively. Equation (5) now becomes

$$\begin{aligned} R_N(\tau_1,\tau_2) = 1 &- \tfrac{1}{2}\cos(\omega_p\tau_1)e^{-\sigma_+^2\tau_1^2/2}e^{-\sigma_-^2\tau_2^2/2} \\ &- \tfrac{1}{2}\cos(\omega_p\tau_2)e^{-\sigma_+^2\tau_2^2/2} - \tfrac{1}{2}e^{-\sigma_-^2\tau_2^2/2} \\ &+ \tfrac{1}{4}\cos[\omega_p(\tau_2+\tau_1)]e^{-\sigma_+^2(\tau_2+\tau_1)^2/2} \\ &+ \tfrac{1}{4}\cos[\omega_p(\tau_2-\tau_1)]e^{-\sigma_+^2(\tau_2-\tau_1)^2/2}. \end{aligned} \quad (6)$$

Equation (6) involves the four timescales, i.e., τ_1, τ_2 and the inverse linewidths $1/\sigma_+$, $1/\sigma_-$. If we set τ_1 to be a fixed value, then Eq. (6) becomes only a function of τ_2. In this case, the last two terms in Eq. (6) correspond to two identical interferograms involving a cosine oscillation with a period of $2\pi/\omega_p$ centered at $\pm\tau_1$. If $\tau_1 < 1/\sigma_+$, these two interferograms will gradually overlap and become fully indistinguishable as τ_1 decreases to be zero. Thus, if one would like to distinguish these two interferograms, τ_1 must be much larger than the inverse linewidth $1/\sigma_+$. If so, the second term in Eq. (6) will tend to be zero. Equation (6) can then be simplified as

$$\begin{aligned} R_N(\tau_1,\tau_2) = 1 &- \tfrac{1}{2}\cos(\omega_p\tau_2)e^{-\sigma_+^2\tau_2^2/2} - \tfrac{1}{2}e^{-\sigma_-^2\tau_2^2/2} \\ &+ \tfrac{1}{4}\cos[\omega_p(\tau_2+\tau_1)]e^{-\sigma_+^2(\tau_2+\tau_1)^2/2} \\ &+ \tfrac{1}{4}\cos[\omega_p(\tau_2-\tau_1)]e^{-\sigma_+^2(\tau_2-\tau_1)^2/2}. \end{aligned} \quad (7)$$

For a fixed value of τ_1, the second term in Eq. (7) represents a cosine oscillation centered at $\tau_2 = 0$ with a temporal width of the envelope that is inversely proportional to the linewidth σ_+ and with an interference visibility of 1/2. The period of the oscillation is determined by the pump center frequency ω_p. The third term in Eq. (7) corresponds to a standard HOM dip centered at $\tau_2 = 0$ with a temporal width that is inversely proportional to the linewidth σ_- and with an interference visibility of 1/2. The last two terms in Eq. (7) correspond to two identical oscillations around $\pm\tau_1$ both with a temporal width of the envelope that is inversely proportional to the linewidth σ_+ and with an interference visibility of 1/4.

If τ_2 is a nonzero constant and $\tau_2 \gg 1/\sigma_+$, Eq. (7) can be further simplified to

$$\begin{aligned} R_N(\tau_1,\tau_2) = 1 &+ \tfrac{1}{4}\cos[\omega_p(\tau_1+\tau_2)]e^{-\sigma_+^2(\tau_2+\tau_1)^2/2} \\ &+ \tfrac{1}{4}\cos[\omega_p(\tau_1-\tau_2)]e^{-\sigma_+^2(\tau_2-\tau_1)^2/2}. \end{aligned} \quad (8)$$

In this case, the coincidence count rate is only the function of τ_1, and the interferogram will only contain two-side oscillations around $\pm\tau_2$ with a temporal width of the envelope that is inversely proportional to the linewidth σ_+.

III. CHARACTERISTIC ANALYSIS OF THE COMBINATION INTERFEROMETER

To understand better the characteristic of the combination interferometer, we give some typical interferograms for different types of frequency correlation based on Eq. (7). Figures 2(a)–2(c) show the typical interferograms for the combination interferometer as a function of $\sigma_+\tau_2$ at $\sigma_+\tau_1 = 5$ for frequency anticorrelated, correlated, and uncorrelated resources, respectively. We can see that the temporal interference patterns associated with biphoton frequency sum and difference can be shown in different parts of an interferogram for all type of frequency entangled resources. It can thus obtain simultaneously the spectral correlation information of biphotons both in frequency sum and frequency by taking the Fourier transform of the upper (green) or lower (orange) envelopes of the interferograms in Fig. 2. Additionally, the interferograms in Fig. 2 contain the information of three timescales, i.e., the temporal width of the envelope of two-side interferograms determined by the inverse linewidth $1/\sigma_+$, the temporal width of the middle dip determined by the inverse linewidth $1/\sigma_-$, and the time interval between two-side interferograms determined by $\pm\tau_1$. It can thus realize the measurement of time intervals on three scales at the same time in a single experiment, which might be useful in quantum metrology. For frequency anticorrelated resource [Fig. 2(a)], the width of frequency difference is much larger than the width of frequency sum, as a result, there is a narrow dip around $\sigma_+\tau_2 = 0$ and a wider envelope of two-side interferograms around $\sigma_+\tau_1 = \pm 5$ due to their inverse dependence with respect to the linewidth of frequency difference and sum, respectively. However, for frequency correlated resource [Fig. 2(b)], the width of frequency sum is much larger than the width of frequency difference, resulting in a wider dip around $\sigma_+\tau_2 = 0$ and a narrow envelope of two-side interferograms around $\sigma_+\tau_1 = \pm 5$. For frequency uncorrelated resource [Fig. 2(c)], the width of frequency sum is

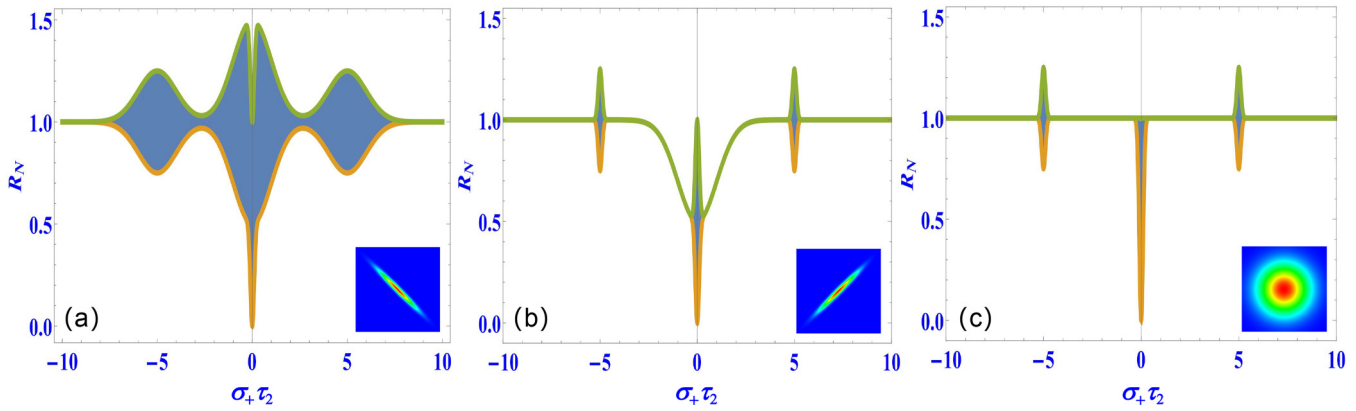

FIG. 2. Typical interferograms of the combination interferometer as a function of $\sigma_+\tau_2$ at $\sigma_+\tau_1 = 5$ for (a) frequency anticorrelated ($\sigma_+/\sigma_- = 0.1$), (b) frequency correlated ($\sigma_+/\sigma_- = 10$), and (c) frequency uncorrelated ($\sigma_+/\sigma_- = 1$) resources. The temporal interference patterns associated with biphoton frequency sum and difference can be shown in different parts of an interferogram for all type of frequency entangled resources. The green and orange curves denote the upper and lower envelopes of the interferograms, respectively. The time delays are in units of the inverse of σ_+. The insets are the corresponding JSIs with the same amplitude of horizontal and vertical coordinates.

identical to the width of frequency difference, resulting in the same width of the middle and the two-side interferograms. Therefore, one can distinguish different types of frequency correlation by only observing a single time-domain quantum interferogram obtained from the combination interferometer. Conversely, one can also characterize different types of frequency correlation by using only a single time-domain quantum interferogram.

To explore the effect of different degree of frequency correlation (the degree of frequency entanglement) on the interferogram, we plot the envelopes of the interferograms as a function of $\sigma_+\tau_2$ at $\sigma_+\tau_1 = 5$ for frequency anticorrelated and frequency correlated resources at different ratios σ_+/σ_-, as shown in Fig. 3. For frequency anticorrelated resource [Fig. 3(a)], the width of the two-side envelopes and the central envelope of R_N above $1/2$ decreases with the increase of ratios σ_+/σ_- (equivalent increase of σ_+), because their widths are only determined by biphoton frequency sum. The central envelope of R_N below $1/2$ remains unchanged due to the same width of biphoton frequency difference. The widths tends to be identical as the ratios increase to be one. For frequency correlated resource [Fig. 3(b)], the width of the two-side envelopes remains unchanged due to the fixed value of σ_-. The central envelope of R_N above $1/2$ increases with the increase of ratios σ_+/σ_- (equivalent decrease of σ_-), because their widths are only determined by biphoton frequency sum. Therefore, one can also determine the degree of frequency entanglement of biphoton source by estimating the ratio σ_+/σ_- obtained from the combination interferometer.

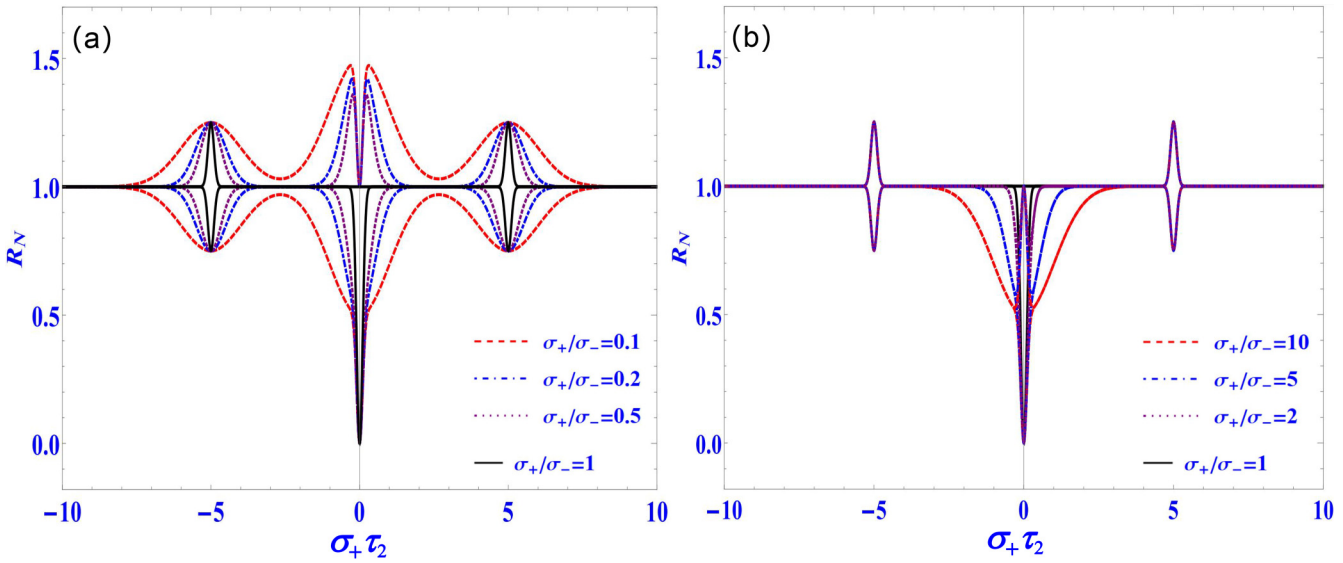

FIG. 3. The envelopes of the interferograms of the combination interferometer as a function of $\sigma_+\tau_2$ at $\sigma_+\tau_1 = 5$ for (a) frequency anticorrelated and (b) frequency correlated resources at different ratios σ_+/σ_-. The black lines correspond to the results of the frequency uncorrelated resources, as a contrast.

IV. DISCUSSION

Based on the combination interferometer, we can build a bridge between a two-dimensional (2D) spectral correlation information of biphotons containing frequency sum and difference and one-dimensional (1D) time-domain interference patterns in a single quantum interferometer. By directly taking Fourier transform of the envelope of an interferogram obtained from the combination interferometer, one can obtain the complete spectral information of biphotons both in frequency sum and difference, i.e., the distributions of $|f_+(\Omega_+)|^2$ and $|f_-(\Omega_-)|^2$. Finally, the JSI can be reconstructed by their product. A direct application of such an interferometer can be found in the field of quantum Fourier-transform spectroscopy [26,32,33], especially for those spectra whose spectral range is not easy to obtain by the conventional spectrograph.

It should be noted that it can be seen from Eqs. (4) and (5) that the results of the time-domain interference of the combination interferometer are only determined by the intensity (not the amplitude) of the biphoton field. This holds for the HOMI and the NOONI, too. It means that these interferometers are not sensitive to the phase of the biphoton field, making it more convenient to measure in an experiment. However, the JSA is sensitive to the phase and is difficult to measure experimentally. If one would like to completely characterize the two-photon state, it is necessary to measure not only the amplitude but also the phase of the biphoton state, as shown in Refs. [34,35].

In the analysis above, we only consider the case of symmetric JSA, but we can see from Eq. (2) that the results of the combination interferometer are different for various symmetry of the JSA. In the HOMI, if the JSA is symmetric, i.e., $f(\omega_s, \omega_i) = f(\omega_i, \omega_s)$, it will result in the bunching effect, a feature associated with bosonic statistics [2]. If the JSA is antisymmetric, i.e., $f(\omega_s, \omega_i) = -f(\omega_i, \omega_s)$, however, this will lead to the antibunching effect, a feature associated with fermionic statistics [36,37]. These effects have been demonstrated in spatial degree of freedom (DOF) [38], frequency DOF [39], and both DOFs of polarization and orbital angular momentum [40]. Also, the influence of the exchange symmetry of the biphoton on the coincidence measurement of both the HOMI and the NOONI has been studied recently in Ref. [41]. For the HOMI, coincidence counts always depend on frequency difference of biphotons, whether the JSA is symmetric, antisymmetric, or anyonic, and a continuous deformation of coincidence counts happens from a dip obtained with a symmetric JSA to a peak obtained with an antisymmetric JSA. However, this is not the case for the NOONI where it depends on biphoton frequency sum for the symmetric JSA but on the frequency difference for the antisymmetric JSA [41]. In our case, the combination interferometer will always depend on both frequency difference and sum whatever the JSA is symmetric or antisymmetric. If the JSA is antisymmetric, the sign of all terms in Eq. (5) except the first constant term will be flipped. Analogously, it can be predicted that the change of the exchange symmetry of the JSA from symmetric to antisymmetric will flip the interferograms in Fig. 2 along $y > 0$ axis at the baseline of $R_N = 1$. Therefore, it is definite that the combination interferometer can be used to completely characterize the spectral features of biphotons for both symmetric and antisymmetric JSA. But for the JSA with anyonic symmetry, the situation will become more complicated. For example, as discussed in Ref. [27], the asymmetry of JSA leads to the degradation of interference visibility in both the HOMI and the NOONI, and the Fourier transform of the interferograms is definitely not corresponding to the spectrum of biphoton frequency sum and difference. A possible way to solve this issue is that we can create a superposition state $\mathcal{F}(\omega_s, \omega_i) = f(\omega_s, \omega_i) + f(\omega_i, \omega_s)$, which satisfies the exchange symmetry condition. Experimentally, this can be realized by placing a nonlinear crystal inside an interferometer, as reported in Ref. [42]. Then, the spectral information with f might be extracted from the one with $\mathcal{F}$. However, for the JSA with anyonic symmetry, the precise relation between the interferogram of the combination interferometer and its Fourier transform may be beyond the scope of the present paper because of the more complex Fourier transform involved, which still needs to be researched further in the future.

Now let us consider another potential application of such an interferometer in generation and characterization of high-dimensional frequency entanglement with the help of the spectrally resolved technology [43,44]. In the spectrally resolved HOM interference, the JSI can be modulated along the axis of frequency difference for a perfectly frequency anticorrelated entangled resource ($\sigma_+ \ll \sigma_-$), and such modulation can discretize continuous frequency entanglement into discrete frequency modes and result in the spectrum with a comb structure in frequency difference direction, which has been proved to be very useful for generating high-dimensional entanglement in frequency-bin qudits [45–47]. On the other hand, in spectrally resolved NOON state interference, it has been demonstrated that the JSI can be modulated along the axis of frequency sum by adjusting the time delay [48,49]. Therefore, it is also possible to generate high-dimensional frequency entanglement using the left part (NOONI) of the combination interferometer in Fig. 1 with the help of spectrally resolved technology. This can be realized by modulating the JSI along the axis of the frequency sum for a perfectly frequency correlated entangled resource ($\sigma_+ \gg \sigma_-$) via adjusting the time delay τ_1. Since the NOONI depends on biphoton frequency sum, which is phase-dependent, the generated high-dimensional frequency entanglement from this way is phase-dependent, too. In principle, a higher-dimensional discrete frequency entanglement can be prepared by increasing the time delay τ_1 and the dimensionality of frequency entanglement (the number of discrete frequency modes) increases with the increase of the time delay τ_1. The dimensionality can be characterized by the change of the Schmidt number. It means that the larger the Schmidt number, the higher the dimensionality. Alternatively, the dimensionality can also be quantified fast by Shannon dimensionality measured through HOM interference, as shown recently in an experiment [50]. Meanwhile, one can use the right part (HOMI) of the combination interferometer in Fig. 1 to directly characterize the generated high-dimensional frequency entanglement according to the time interval $2\tau_1$ between two-side temporal interferograms. It means that the larger the time interval $2\tau_1$, the higher the dimensionality of frequency entanglement.

V. CONCLUSIONS

We have proposed a combination interferometer that always depends on both biphoton frequency sum and difference whatever the exchange symmetry of biphotons. This interferometer combined the advantages of both the NOONI that depends only on biphoton frequency sum and the HOMI that depends only on biphoton frequency difference into a single interferometer. It can thus simultaneously obtain the spectral correlation information of biphotons in both frequency sum and difference by taking the Fourier transform from a single time-domain quantum interferogram, which provides a method for complete spectral characterization of an arbitrary two-photon state with exchange symmetry. A direct application of such an interferometer can be found in quantum Fourier-transform spectroscopy, where direct spectral measurement is difficult. The typical interferograms for different types of frequency correlation have been presented to show the characteristic of the combination interferometer. Furthermore, as it can realize the measurement of time intervals on three scales at the same time, we expect that it can provide a method in quantum metrology. Finally, as a potential application, we have shown that it is also possible to generate high-dimensional and phase-controlled frequency entanglement in such an interferometer with spectrally resolved technology by adjusting the time delay and characterize it directly with the two-side oscillations that appear in a temporal interferogram.

ACKNOWLEDGMENTS

This work has been supported by National Natural Science Foundation of China (Grants No. 12074309, No. 12074299, No. 12033007, No. 61875205, No. 12103058, and No. 61801458), the Youth Innovation Team of Shaanxi Universities, and the Natural Science Foundation of Hubei Province (Grant No. 2022CFA039).

APPENDIX A: THE COINCIDENCE COUNT RATES FOR THE COMBINATION INTERFEROMETER DERIVED FROM THE FREQUENCY DOMAIN

In this section, we deduce the equations for the combination interferometer in Fig. 1 from the frequency domain. The two-photon state from a SPDC process can be described as

$$|\Psi\rangle = \iint d\omega_s d\omega_i f(\omega_s,\omega_i)\hat{a}_s^{\dagger}(\omega_s)\hat{a}_i^{\dagger}(\omega_i)|0\rangle, \tag{A1}$$

where ω is the angular frequency, and $\hat{a}_{s,i}^{\dagger}$ is the creation operator and the subscripts s and i denote the signal and idler photons from SPDC, respectively. $|0\rangle$ stands for a vacuum state. $f(\omega_s,\omega_i)$ is the JSA of the signal and idler photons.

The detection field operators of detector 5 (D5) and detector 6 (D6) are

$$\hat{E}_5^{(+)}(t_5) = \frac{1}{\sqrt{2\pi}}\int_0^{\infty} d\omega_5 \hat{a}_5(\omega_5)e^{-i\omega_5 t_5}, \tag{A2}$$

$$\hat{E}_6^{(+)}(t_6) = \frac{1}{\sqrt{2\pi}}\int_0^{\infty} d\omega_6 \hat{a}_6(\omega_6)e^{-i\omega_6 t_6}, \tag{A3}$$

where the subscripts 5 and 6 denote the photons detected by D5 and D6, respectively. The transformation rule of the 50/50 beam splitter (BS3) is

$$\hat{a}_5(\omega_5) = [\hat{a}_3(\omega_5)e^{-i\omega_5\tau_2} + \hat{a}_4(\omega_5)]/\sqrt{2}, \tag{A4}$$

$$\hat{a}_6(\omega_6) = [\hat{a}_3(\omega_6)e^{-i\omega_6\tau_2} - \hat{a}_4(\omega_6)]/\sqrt{2}. \tag{A5}$$

The transformation rule of the 50/50 BS2 is

$$\hat{a}_3(\omega_5) = [\hat{a}_1(\omega_5)e^{-i\omega_5\tau_1} + \hat{a}_2(\omega_5)]/\sqrt{2}, \tag{A6}$$

$$\hat{a}_4(\omega_6) = [\hat{a}_1(\omega_6)e^{-i\omega_6\tau_1} - \hat{a}_2(\omega_6)]/\sqrt{2}. \tag{A7}$$

The transformation rule of the 50/50 BS1 is

$$\begin{aligned}\hat{a}_1(\omega_5) &= [\hat{a}_s(\omega_5) + \hat{a}_i(\omega_5)]/\sqrt{2},\\ \hat{a}_2(\omega_5) &= [\hat{a}_s(\omega_5) - \hat{a}_i(\omega_5)]/\sqrt{2},\end{aligned} \tag{A8}$$

$$\begin{aligned}\hat{a}_1(\omega_6) &= [\hat{a}_s(\omega_6) + \hat{a}_i(\omega_6)]/\sqrt{2},\\ \hat{a}_2(\omega_6) &= [\hat{a}_s(\omega_6) - \hat{a}_i(\omega_6)]/\sqrt{2}.\end{aligned} \tag{A9}$$

So, we have

$$\hat{a}_3(\omega_5) = [(\hat{a}_s(\omega_5) + \hat{a}_i(\omega_5))e^{-i\omega_5\tau_1} + (\hat{a}_s(\omega_5) - \hat{a}_i(\omega_5))]/2, \tag{A10}$$

$$\hat{a}_4(\omega_5) = [(\hat{a}_s(\omega_5) + \hat{a}_i(\omega_5))e^{-i\omega_5\tau_1} - (\hat{a}_s(\omega_5) - \hat{a}_i(\omega_5))]/2, \tag{A11}$$

$$\hat{a}_3(\omega_6) = [(\hat{a}_s(\omega_6) + \hat{a}_i(\omega_6))e^{-i\omega_6\tau_1} + (\hat{a}_s(\omega_6) - \hat{a}_i(\omega_6))]/2, \tag{A12}$$

$$\hat{a}_4(\omega_6) = [(\hat{a}_s(\omega_6) + \hat{a}_i(\omega_6))e^{-i\omega_6\tau_1} - (\hat{a}_s(\omega_6) - \hat{a}_i(\omega_6))]/2. \tag{A13}$$

Substituting Eqs. (A10)–(A13) into Eqs. (A4) and (A5), we have

$$\begin{aligned}\hat{a}_5(\omega_5) = [&\hat{a}_s(\omega_5)(e^{-i\omega_5(\tau_1+\tau_2)} + e^{-i\omega_5\tau_1} + e^{-i\omega_5\tau_2} - 1)\\ &+ \hat{a}_i(\omega_5)(e^{-i\omega_5(\tau_1+\tau_2)} + e^{-i\omega_5\tau_1} - e^{-i\omega_5\tau_2} + 1)]/\\ &2\sqrt{2},\end{aligned} \tag{A14}$$

$$\begin{aligned}\hat{a}_6(\omega_6) = [&\hat{a}_s(\omega_6)(e^{-i\omega_6(\tau_1+\tau_2)} + e^{-i\omega_6\tau_2} - e^{-i\omega_6\tau_1} + 1)\\ &+ \hat{a}_i(\omega_6)(e^{-i\omega_6(\tau_1+\tau_2)} - e^{-i\omega_6\tau_2} - e^{-i\omega_6\tau_1} - 1)]/\\ &2\sqrt{2},\end{aligned} \tag{A15}$$

The coincidence count rates between two detectors as functions of delay time τ_1, τ_2 can be expressed as

$$\begin{aligned}R(\tau_1,\tau_2) &= \iint dt_5 dt_6 \langle\Psi|\hat{E}_5^{(-)}\hat{E}_6^{(-)}\hat{E}_6^{(+)}\hat{E}_5^{(+)}|\Psi\rangle\\ &= \iint dt_5 dt_6 |\langle 0|\hat{E}_6^{(+)}\hat{E}_5^{(+)}|\Psi\rangle|^2.\end{aligned} \tag{A16}$$

Consider $\hat{E}_6^{(+)}\hat{E}_5^{(+)}|\Psi\rangle$; only two out of four terms exist. The first term is

$$\begin{aligned}
&\frac{1}{16\pi}\iint d\omega_5 d\omega_6 \hat{a}_s(\omega_5)\hat{a}_i(\omega_6)e^{-i\omega_5 t_5}e^{-i\omega_6 t_6}(e^{-i\omega_5(\tau_1+\tau_2)}+e^{-i\omega_5\tau_1}+e^{-i\omega_5\tau_2}-1)\\
&\quad\times(e^{-i\omega_6(\tau_1+\tau_2)}-e^{-i\omega_6\tau_2}-e^{-i\omega_6\tau_1}-1)\iint d\omega_s d\omega_i f(\omega_s,\omega_i)\hat{a}_s^\dagger(\omega_s)\hat{a}_i^\dagger(\omega_i)|0\rangle\\
&=\frac{1}{16\pi}\iint d\omega_5 d\omega_6 e^{-i\omega_5 t_5}e^{-i\omega_6 t_6}f(\omega_5,\omega_6)(e^{-i\omega_5(\tau_1+\tau_2)}+e^{-i\omega_5\tau_1}+e^{-i\omega_5\tau_2}-1)\\
&\quad\times(e^{-i\omega_6(\tau_1+\tau_2)}-e^{-i\omega_6\tau_2}-e^{-i\omega_6\tau_1}-1)|0\rangle.
\end{aligned}\tag{A17}$$

In this calculation, the relationships $\hat{a}_5(\omega_5)\hat{a}_s^\dagger(\omega_s)=\delta(\omega_5-\omega_s)$, $\hat{a}_i(\omega_6)\hat{a}_i^\dagger(\omega_i)=\delta(\omega_6-\omega_i)$ are used. The second term is

$$\begin{aligned}
&\frac{1}{16\pi}\iint d\omega_6 d\omega_5 \hat{a}_s(\omega_6)\hat{a}_i(\omega_5)e^{-i\omega_6 t_6}e^{-i\omega_5 t_5}(e^{-i\omega_6(\tau_1+\tau_2)}+e^{-i\omega_6\tau_2}-e^{-i\omega_6\tau_1}+1)\\
&\quad\times(e^{-i\omega_5(\tau_1+\tau_2)}-e^{-i\omega_5\tau_2}+e^{-i\omega_5\tau_1}+1)\iint d\omega_s d\omega_i f(\omega_s,\omega_i)\hat{a}_s^\dagger(\omega_s)\hat{a}_i^\dagger(\omega_i)|0\rangle\\
&=\frac{1}{16\pi}\iint d\omega_6 d\omega_5 e^{-i\omega_6 t_6}e^{-i\omega_5 t_5}f(\omega_6,\omega_5)(e^{-i\omega_6(\tau_1+\tau_2)}+e^{-i\omega_6\tau_2}-e^{-i\omega_6\tau_1}+1)\\
&\quad\times(e^{-i\omega_5(\tau_1+\tau_2)}-e^{-i\omega_5\tau_2}+e^{-i\omega_5\tau_1}+1)|0\rangle.
\end{aligned}\tag{A18}$$

Combine these two terms:

$$\begin{aligned}
\hat{E}_6^{(+)}\hat{E}_5^{(+)}|\Psi\rangle=\frac{1}{16\pi}\iint d\omega_1 d\omega_2 e^{-i\omega_5 t_5}e^{-i\omega_6 t_6}[&f(\omega_5,\omega_6)(e^{-i\omega_5(\tau_1+\tau_2)}+e^{-i\omega_5\tau_1}+e^{-i\omega_5\tau_2}-1)\\
&\times(e^{-i\omega_6(\tau_1+\tau_2)}-e^{-i\omega_6\tau_1}-e^{-i\omega_6\tau_2}-1)+f(\omega_6,\omega_5)(e^{-i\omega_6(\tau_1+\tau_2)}+e^{-i\omega_6\tau_2}-e^{-i\omega_6\tau_1}+1)\\
&\times(e^{-i\omega_5(\tau_1+\tau_2)}-e^{-i\omega_5\tau_2}+e^{-i\omega_5\tau_1}+1)]|0\rangle.
\end{aligned}\tag{A19}$$

Then,

$$\begin{aligned}
\langle\Psi|\hat{E}_5^{(-)}\hat{E}_6^{(-)}\hat{E}_6^{(+)}\hat{E}_5^{(+)}|\Psi\rangle=\left(\frac{1}{16\pi}\right)^2\iint d\omega_5' d\omega_6' e^{-i\omega_5' t_5}e^{-i\omega_6' t_6}[&f^*(\omega_6',\omega_5')(e^{i\omega_6'(\tau_1+\tau_2)}+e^{i\omega_6'\tau_2}-e^{i\omega_6'\tau_1}+1)\\
&\times(e^{i\omega_5'(\tau_1+\tau_2)}-e^{i\omega_5'\tau_2}+e^{i\omega_5'\tau_1}+1)+f^*(\omega_5',\omega_6')(e^{i\omega_5'(\tau_1+\tau_2)}+e^{i\omega_5'\tau_1}+e^{i\omega_5'\tau_2}-1)\\
&\times(e^{i\omega_6'(\tau_1+\tau_2)}-e^{i\omega_6'\tau_1}-e^{i\omega_6'\tau_2}-1)]\left(\frac{1}{16\pi}\right)^2\iint d\omega_5 d\omega_6 e^{-i\omega_5 t_5}e^{-i\omega_6 t_6}\\
&\times[f(\omega_6,\omega_5)(e^{-i\omega_6(\tau_1+\tau_2)}+e^{-i\omega_6\tau_2}-e^{-i\omega_6\tau_1}+1)(e^{-i\omega_5(\tau_1+\tau_2)}-e^{-i\omega_5\tau_2}+e^{-i\omega_5\tau_1}+1)\\
&+f(\omega_5,\omega_6)(e^{-i\omega_5(\tau_1+\tau_2)}+e^{-i\omega_5\tau_1}+e^{-i\omega_5\tau_2}-1)(e^{-i\omega_6(\tau_1+\tau_2)}-e^{-i\omega_6\tau_1}-e^{-i\omega_6\tau_2}-1)].
\end{aligned}\tag{A20}$$

Finally,

$$\begin{aligned}
R(\tau_1,\tau_2)=\iint dt_5 dt_6\langle\Psi|\hat{E}_5^{(-)}\hat{E}_6^{(-)}\hat{E}_6^{(+)}\hat{E}_5^{(+)}|\Psi\rangle&=\left(\frac{1}{16\pi}\right)^2\iint d\omega_5 d\omega_6 d\omega_5' d\omega_6'\delta(\omega_5-\omega_5')\delta(\omega_6-\omega_6')\\
&\times[f^*(\omega_6',\omega_5')(e^{i\omega_6'(\tau_1+\tau_2)}+e^{i\omega_6'\tau_2}-e^{i\omega_6'\tau_1}+1)(e^{i\omega_5'(\tau_1+\tau_2)}-e^{i\omega_5'\tau_2}+e^{i\omega_5'\tau_1}+1)\\
&+f^*(\omega_5',\omega_6')(e^{i\omega_5'(\tau_1+\tau_2)}+e^{i\omega_5'\tau_1}+e^{i\omega_5'\tau_2}-1)(e^{i\omega_6'(\tau_1+\tau_2)}-e^{i\omega_6'\tau_1}-e^{i\omega_6'\tau_2}-1)]\\
&\times[f(\omega_6,\omega_5)(e^{-i\omega_6(\tau_1+\tau_2)}+e^{-i\omega_6\tau_2}-e^{-i\omega_6\tau_1}+1)(e^{-i\omega_5(\tau_1+\tau_2)}-e^{-i\omega_5\tau_2}+e^{-i\omega_5\tau_1}+1)\\
&+f(\omega_5,\omega_6)(e^{-i\omega_5(\tau_1+\tau_2)}+e^{-i\omega_5\tau_1}+e^{-i\omega_5\tau_2}-1)(e^{-i\omega_6(\tau_1+\tau_2)}-e^{-i\omega_6\tau_1}-e^{-i\omega_6\tau_2}-1)]\\
&=\frac{1}{64}\iint d\omega_5 d\omega_6|f(\omega_6,\omega_5)(e^{-i\omega_6(\tau_1+\tau_2)}+e^{-i\omega_6\tau_2}-e^{-i\omega_6\tau_1}+1)(e^{-i\omega_5(\tau_1+\tau_2)}-e^{-i\omega_5\tau_2}+e^{-i\omega_5\tau_1}+1)\\
&+f(\omega_5,\omega_6)(e^{-i\omega_5(\tau_1+\tau_2)}+e^{-i\omega_5\tau_1}+e^{-i\omega_5\tau_2}-1)(e^{-i\omega_6(\tau_1+\tau_2)}-e^{-i\omega_6\tau_1}-e^{-i\omega_6\tau_2}-1)|^2.
\end{aligned}\tag{A21}$$

In above calculation, the relationship of $\delta(\omega-\omega') = \frac{1}{2\pi}\int_{-\infty}^{\infty} e^{i(\omega-\omega')t}dt$ is used. f^* is the complex conjugate of f. To introduce fewer variables, Eq. (A21) can be rewritten as

$$R(\tau_1,\tau_2) = \frac{1}{64}\int_0^{\infty}\int_0^{\infty} d\omega_s d\omega_i r(\omega_s,\omega_i,\tau_1,\tau_2). \tag{A22}$$

This is Eq. (1) in the main text.

APPENDIX B: THE COINCIDENCE COUNT RATES FOR THE COMBINATION INTERFEROMETER DERIVED FROM THE TIME DOMAIN

To obtain the temporal expression of coincidence count rates, we need to take the Fourier transform of Eq. (A21) back into the time representation, yielding to the JTI

$$\begin{aligned}|\Psi(t_s,t_i)|^2 = |&A_1(t_s,t_i) - A_2(t_s+\tau_1,t_i+\tau_1) + A_3(t_s,t_i+\tau_2) - A_4(t_s+\tau_2,t_i) + A_5(t_s+\tau_1,t_i+[\tau_1+\tau_2])\\ &- A_6(t_s+[\tau_1+\tau_2],t_i+\tau_1) + A_7(t_s+[\tau_1+\tau_2],t_i+[\tau_1+\tau_2]) - A_8(t_s+\tau_2,t_i+\tau_2)|^2,\end{aligned} \tag{B1}$$

where Ψ is called as effective two-photon wave function. A denotes the quantum-mechanical probability amplitude for the coincidence detection event and can be obtained from the Fourier transform of the JSA at the coordinates marked in Eq. (B1). After taking the module squared of Eq. (B1), the JTI has 64 terms,

$$\begin{aligned}|\Psi(t_s,t_i)|^2 = {}&|A_1|^2+|A_2|^2+|A_3|^2+|A_4|^2+|A_5|^2+|A_6|^2+|A_7|^2+|A_8|^2\\ &+A_1^*A_3+A_1A_3^*+A_1^*A_5+A_1A_5^*+A_1^*A_7+A_1A_7^*+A_2^*A_4+A_2A_4^*+A_2^*A_6+A_2A_6^*+A_2^*A_8+A_2A_8^*\\ &+A_3^*A_5+A_3A_5^*+A_3^*A_7+A_3A_7^*+A_4^*A_6+A_4A_6^*+A_4^*A_8+A_4A_8^*+A_5^*A_7+A_5A_7^*+A_6^*A_8+A_6A_8^*\\ &-A_1^*A_2-A_1A_2^*-A_1^*A_4-A_1A_4^*-A_1^*A_6-A_1A_6^*-A_1^*A_8-A_1A_8^*-A_2^*A_3-A_2A_3^*-A_2^*A_5-A_2A_5^*\\ &-A_2^*A_7-A_2A_7^*-A_3^*A_4-A_3A_4^*-A_3^*A_6-A_3A_6^*-A_3^*A_8-A_3A_8^*-A_4^*A_5-A_4A_5^*-A_4^*A_7-A_4A_7^*\\ &-A_5^*A_6-A_5A_6^*-A_5^*A_8-A_5A_8^*-A_6^*A_7-A_6A_7^*-A_7^*A_8-A_7A_8^*.\end{aligned} \tag{B2}$$

Then, the coincidence count rates between two detectors as functions of delay time τ_1, τ_2 can be rewritten as

$$R(\tau_1,\tau_2) = \int_{-\infty}^{\infty}\int_{-\infty}^{\infty} dt_s dt_i |\Psi(t_s,t_i)|^2. \tag{B3}$$

As an example, we take the JSA as the product of two Gaussian functions,

$$f(\omega_s,\omega_i) = \exp\left(-\frac{(\omega_s+\omega_i-\omega_p)^2}{4\sigma_+^2}\right)\exp\left(-\frac{(\omega_s-\omega_i)^2}{4\sigma_-^2}\right). \tag{B4}$$

Taking the Fourier transform of Eq. (B4) at the coordinates marked in Eq. (B1) and integrating the first eight terms in Eq. (B2) over the entire time range, we can obtain a normalized factor $8\pi\sigma_+\sigma_-$. Similarly, integrating $-A_3^*A_6 - A_3A_6^* - A_4^*A_5 - A_4A_5^*$, $-A_1^*A_8 - A_1A_8^* - A_2^*A_7 - A_2A_7^*$, $-A_3^*A_4 - A_3A_4^* - A_5^*A_6 - A_5A_6^*$, and $A_1^*A_7 + A_1A_7^* + A_2^*A_8 + A_2A_8^*$ in Eq. (B2), we can obtain the normalized results, which correspond to the second, the third, the fourth and the last two terms in Eq. (5), respectively. The remaining terms in Eq. (B2) have no contributions to the integral of Eq. (B3). We therefore obtain the same result from the time domain as Eq. (5) derived from the frequency domain.

APPENDIX C: THE COINCIDENCE COUNT RATES FOR THE HOMI AND THE NOONI

To compare the results of the HOMI and the NOONI with the combination interferometer, we give the coincidence count rates of these two interferometers as follows (see details in Ref. [24]):

$$R_{\pm}(\tau) \sim \int_0^{\infty}\int_0^{\infty} d\omega_s d\omega_i r_{\pm}(\omega_s,\omega_i,\tau), \tag{C1}$$

where

$$r_+(\omega_s,\omega_i,\tau) = |f(\omega_i,\omega_s)(e^{-i\omega_i\tau}+1)(e^{-i\omega_s\tau}+1) + f(\omega_s,\omega_i)(e^{-i\omega_s\tau}-1)(e^{-i\omega_i\tau}-1)|^2, \tag{C2}$$

$$r_-(\omega_s,\omega_i,\tau) = |f(\omega_i,\omega_s)e^{-i\omega_s\tau} - f(\omega_s,\omega_i)e^{-i\omega_i\tau}|^2. \tag{C3}$$

The subscripts "+" and "−" correspond to a NOON state and a standard HOM interferometer, respectively. If the JSA is symmetric, i.e., $f(\omega_s,\omega_i) = f(\omega_i,\omega_s)$, we can further rewrite the above equation as

$$r_{\pm}(\omega_s,\omega_i,\tau) = |f(\omega_s,\omega_i)|^2[1\pm\cos(\omega_s\pm\omega_i)\tau]. \tag{C4}$$

If the JSA is antisymmetric, i.e., $f(\omega_s, \omega_i) = -f(\omega_i, \omega_s)$, we have

$$r_+(\omega_s, \omega_i, \tau) = r_-(\omega_s, \omega_i, \tau) = |f(\omega_s, \omega_i)|^2[1 + \cos(\omega_s - \omega_i)\tau]. \tag{C5}$$

[1] J.-W. Pan, Z.-B. Chen, C.-Y. Lu, H. Weinfurter, A. Zeilinger, and M. Żukowski, Multiphoton entanglement and interferometry, Rev. Mod. Phys. **84**, 777 (2012).

[2] C. K. Hong, Z. Y. Ou, and L. Mandel, Measurement of Subpicosecond Time Intervals between Two Photons by Interference, Phys. Rev. Lett. **59**, 2044 (1987).

[3] F. Bouchard, A. Sit, Y. Zhang, R. Fickler, F. M. Miatto, Y. Yao, F. Sciarrino, and E. Karimi, Two-photon interference: The Hong–Ofu–Mandel effect, Rep. Prog. Phys. **84**, 012402 (2021).

[4] A. N. Boto, P. Kok, D. S. Abrams, S. L. Braunstein, C. P. Williams, and J. P. Dowling, Quantum Interferometric Optical Lithography: Exploiting Entanglement to Beat the Diffraction Limit, Phys. Rev. Lett. **85**, 2733 (2000).

[5] Z. Y. Ou and L. Mandel, Violation of Bell's Inequality and Classical Probability in a Two-Photon Correlation Experiment, Phys. Rev. Lett. **61**, 50 (1988).

[6] A. M. Steinberg, P. G. Kwiat, and R. Y. Chiao, Dispersion cancellation and high-resolution time measurements in a fourth order optical interferometer, Phys. Rev. A **45**, 6659 (1992).

[7] O. Minaeva, C. Bonato, B. E. A. Saleh, D. S. Simon, and A. V. Sergienko, Odd- and Even-Order Dispersion Cancellation in Quantum Interferometry, Phys. Rev. Lett. **102**, 100504 (2009).

[8] J. Ryu, K. Cho, C.-H. Oh, and H. Kang, All-order dispersion cancellation and energy-time entangled state, Opt. Express **25**, 1360 (2017).

[9] N. Gisin and R. Thew, Quantum communication, Nat. Photon. **1**, 165 (2007).

[10] T. D. Ladd, F. Jelezko, R. Laflamme, Y. Nakamura, C. Monroe, and J. L. O'Brien, Quantum computers, Nature (London) **464**, 45 (2010).

[11] Y. H. Shih, Quantum imaging, IEEE J. Sel. Top. Quantum Electron. **13**, 1016 (2007).

[12] P.-A. Moreau, E. Toninelli, T. Gregory, and M. J. Padgett, Imaging with quantum states of light, Nat. Rev. Phys. **1**, 367 (2019).

[13] B. Bell, S. Kannan, A. McMillan, A. S. Clark, W. J. Wadsworth, and J. G. Rarity, Multicolor Quantum Metrology with Entangled Photons, Phys. Rev. Lett. **111**, 093603 (2013).

[14] Y. Chen, L. Hong, and L. Chen, Quantum interferometric metrology with entangled photons, Front. Phys. **10**, 892519 (2022).

[15] A. Lyons, G. C. Knee, E. Bolduc, T. Roger, J. Leach, E. M. Gauger, and D. Faccio, Attosecond-resolution Hong-Ou-Mandel interferometry, Sci. Adv. **4**, eaap9416 (2018).

[16] K. Edamatsu, R. Shimizu, and T. Itoh, Measurement of the Photonic de Broglie Wavelength of Entangled Photon Pairs Generated by Spontaneous Parametric Down-Conversion, Phys. Rev. Lett. **89**, 213601 (2002).

[17] M. W. Mitchell, J. S. Lundeen, and A. M. Steinberg, Super-resolving phase measurements with a multiphoton entangled state, Nature (London) **429**, 161 (2004).

[18] V. Giovannetti, S. Lloyd, and L. Maccone, Quantum-enhanced measurements: Beating the standard quantum limit, Science **306**, 1330 (2004).

[19] T. Nagata, R. Okamoto, J. O'Brien, K. Sasaki, and S. Takeuchi, Beating the standard quantum limit with four-entangled photons, Science **316**, 726 (2007).

[20] T. Ono, R. Okamoto, and S. Takeuchi, An entanglement-enhanced microscope, Nat. Commun. **4**, 2426 (2013).

[21] Y. Israel, S. Rosen, and Y. Silberberg, Supersensitive Polarization Microscopy Using NOON States of Light, Phys. Rev. Lett. **112**, 103604 (2014).

[22] R. B. Jin, M. Fujiwara, R. Shimizu, R. J. Collins, G. S. Buller, T. Yamashita, S. Miki, H. Terai, M. Takeoka, and M. Sasaki, Detection dependent six-photon Holland-Burnett state interference, Sci. Rep. **6**, 36914 (2016).

[23] M. Bergmann and P. van Loock, Quantum error correction against photon loss using NOON states, Phys. Rev. A **94**, 012311 (2016).

[24] R.-B. Jin and R. Shimizu, Extended wiener–Khinchin theorem for quantum spectral analysis, Optica **5**, 93 (2018).

[25] H. Seki, K. Miyajima, and R. Shimizu, Quantum interferometric spectroscopy of a biexciton, Phys. Rev. A **106**, 063716 (2022).

[26] Y. Chen and L. Chen, Quantum Wiener-Khinchin Theorem for Spectral-Domain Optical Coherence Tomography, Phys. Rev. Appl. **18**, 014077 (2022).

[27] V. Giovannetti, L. Maccone, J. H. Shapiro, and F. N. C. Wong, Extended phase-matching conditions for improved entanglement generation, Phys. Rev. A **66**, 043813 (2002).

[28] A. F. Abouraddy, T. M. Yarnall, and G. Di Giuseppe, Phase-unlocked Hong-Ou-Mandel interferometry, Phys. Rev. A **87**, 062106 (2013).

[29] J.-P. W. MacLean, J. M. Donohue, and K. J. Resch, Direct Characterization of Ultrafast Energy-Time Entangled Photon Pairs, Phys. Rev. Lett. **120**, 053601 (2018).

[30] R.-B. Jin, T. Saito, and R. Shimizu, Time-Frequency Duality of Biphotons for Quantum Optical Synthesis, Phys. Rev. Appl. **10**, 034011 (2018).

[31] K. Zielnicki, K. Garay-Palmett, D. Cruz-Delgado, H. Cruz-Ramirez, M. F. O'Boyle, B. Fang, V. O. Lorenz, A. B. U'Ren, and P. G. Kwiat, Joint spectral characterization of photon-pair sources, J. Mod. Opt. **65**, 1141 (2018).

[32] Y. Mukai, M. Arahata, T. Tashima, R. Okamoto, and S. Takeuchi, Quantum Fourier-Transform Infrared Spectroscopy for Complex Transmittance Measurements, Phys. Rev. Appl. **15**, 034019 (2021).

[33] Y. Mukai, R. Okamoto, and S. Takeuchi, Quantum Fourier-transform infrared spectroscopy in the fingerprint region, Opt. Express **30**, 22624 (2022).

[34] J.-P. W. MacLean, S. Schwarz, and K. J. Resch, Reconstructing ultrafast energy-time-entangled two-photon pulses, Phys. Rev. A **100**, 033834 (2019).

[35] A. O. C. Davis, V. Thiel, and B. J. Smith, Measuring the quantum state of a photon pair entangled in frequency and time, Optica **7**, 1317 (2020).

[36] J. Peřina, Jr., M. Centini, C. Sibilia, M. Bertolotti, and M. Scalora, Antisymmetric entangled two-photon states generated in nonlinear GaN/AlN photonic-band-gap structures, Phys. Rev. A **75**, 013805 (2007).

[37] A. Fedrizzi, T. Herbst, M. Aspelmeyer, M. Barbieri, T. Jennewein, and A. Zeilinger, Anti-symmetrization reveals hidden entanglement, New J. Phys. **11**, 103052 (2009).

[38] S. P. Walborn, A. N. de Oliveira, S. Pádua, and C. H. Monken, Multimode Hong-Ou-Mandel Interference, Phys. Rev. Lett. **90**, 143601 (2003).

[39] S. Francesconi, F. Baboux, A. Raymond, N. Fabre, G. Boucher, A. Lemaître, P. Milman, M. Amanti, and S. Ducci, Engineering two-photon wavefunction and exchange statistics in a semiconductor chip, Optica **7**, 316 (2020).

[40] Z.-F. Liu, C. Chen, J.-M. Xu, Z.-M. Cheng, Z.-C. Ren, B.-W. Dong, Y.-C. Lou, Y.-X. Yang, S.-T. Xue, Z.-H. Liu, W.-Z. Zhu, X.-L. Wang, and H.-T. Wang, Hong-Ou-Mandel Interference between Two Hyperentangled Photons Enables Observation of Symmetric and Antisymmetric Particle Exchange Phases, Phys. Rev. Lett. **129**, 263602 (2022).

[41] N. Fabre, Interferometric signature of different spectral symmetries of biphoton states, Phys. Rev. A **105**, 053716 (2022).

[42] O. Kuzucu and F. N. C. Wong, Pulsed Sagnac source of narrowband polarization-entangled photons, Phys. Rev. A **77**, 032314 (2008).

[43] T. Gerrits, F. Marsili, V. B. Verma, L. K. Shalm, M. Shaw, R. P. Mirin, and S. W. Nam, Spectral correlation measurements at the Hong-Ou-Mandel interference dip, Phys. Rev. A **91**, 013830 (2015).

[44] R.-B. Jin, T. Gerrits, M. Fujiwara, R. Wakabayashi, T. Yamashita, S. Miki, H. Terai, R. Shimizu, M. Takeoka, and M. Sasaki, Spectrally resolved Hong-Ou-Mandel interference between independent photon sources, Opt. Express **23**, 28836 (2015).

[45] R.-B. Jin, R. Shimizu, M. Fujiwara, M. Takeoka, R. Wakabayashi, T. Yamashita, S. Miki, H. Terai, T. Gerrits, and M. Sasaki, Simple method of generating and distributing frequency-entangled qudits, Quantum Sci. Technol. **1**, 015004 (2016).

[46] Y. Chen, S. Ecker, L. Chen, F. Steinlechner, M. Huber, and R. Ursin, Temporal distinguishability in Hong-Ou-Mandel interference: Generation and characterization of high-dimensional frequency entanglement, npj Quantum Inf. **7**, 167 (2021).

[47] B. Li, B. Yuan, C. Chen, X. Xiang, R. Quan, R. Dong, S. Zhang, and R.-B. Jin, Spectrally resolved two-photon interference in a modified Hong–Ou–Mandel interferometer, Opt. Laser Technol. **159**, 109039 (2023).

[48] V. V. Orre, E. A. Goldschmidt, A. Deshpande, A. V. Gorshkov, V. Tamma, M. Hafezi, and S. Mittal, Interference of Temporally Distinguishable Photons Using Frequency-Resolved Detection, Phys. Rev. Lett. **123**, 123603 (2019).

[49] R.-B. Jin, R. Shimizu, T. Ono, M. Fujiwara, G.-W. Deng, Q. Zhou, M. Sasaki, and M. Takeoka, Spectrally resolved NOON state interference, arXiv:2104.01062.

[50] L. Hong, Y. Zhang, Y. Chen, and L. Chen, Fast quantifier of high-dimensional frequency entanglement through Hong–Ou–Mandel interference, Adv. Quantum Technol. **6**, 2300012 (2023).